A Slightly Deformable Darcy Drop in Linear Flows

Y.-N. Young[1], Yoichiro Mori[2] and Michael J. Miksis[3]
[1]*Department of Mathematical Sciences,*
New Jersey Institute of Technology, Newark, New Jersey, 07102, USA
[2]*Department of Mathematics, University of Minnesota,*
Minneapolis, Minnesota, 55455, USA
[3]*Department of Engineering Sciences and Applied Mathematics,*
Northwestern University, Evanston, Illinois, 60208, USA
(Dated: October 22, 2018)

Abstract

The small-deformation of a poroelastic drop due to an external linear flow field in the suspending medium is investigated. A two-phase flow model is developed to study the small-deformation of such a poroelastic drop under linear flows. Inside the drop a deformable porous network with a bending rigidity and a viscosity is fully immersed in a viscous fluid. When the viscous dissipation of the interior fluid phase is negligible (compared to the friction between the fluid and the skeleton), the two-phase flow is reduced to a poroelastic Darcy fluid with a deformable porous network. At the interface between the poroelastic drop and the exterior Stokesian fluid, a novel set of boundary conditions are derived by the free energy dissipation principle. Both slip and permeability are taken into account and the permeating flow induces dissipation that depends on the elastic stress of the interior solid. Assuming that the porous network is slightly deformed from its original spherical shape due to its large bending rigidity, a small-deformation analysis is conducted. A steady equilibrium is computed for two different linear flows: a uniaxial extensional flow and a planar shear flow. By exploring the interfacial slip, permeability and network elasticity various flow patterns are found at equilibrium of these slightly deformed poroelastic drops. Linear dynamics of the small-amplitude deviation of the poroelastic drop from the spherical shape is governed by a nonlinear eigenvalue problem, and the eigenvalues are determined numerically, and asymptotically in certain limits. These results lay the foundation for studying the rheology of a suspension of poroelastic spherical particles, and give insight to possible flow patterns of a system of self-propelling swimmers with porous flow (such as intracellular cytosol) inside.

PACS numbers: Valid PACS appear here

I. INTRODUCTION

Flow in porous media is of significant relevance to many research areas that range from turbulent transport through porous media in geophysics, filtration in hydrology, to cell and tissue mechanics in bio-mechanical engineering. A great deal of effort has been devoted to the modeling of pressure-driven fluid flow, thermal convection and propagation of sound waves in porous media, and the fluid pressure in water-filled connective tissues such as the cornea. Depending on the specific applications, the porous structures may be treated either as rigid and non-deformable in hydrology of filtration, or they may deform as their dynamics is coupled to the fluid flow around them in tissue mechanics.

When the porous medium consists of a rigid skeleton of a fixed shape and distribution, the steady flow of the surrounding viscous fluid has been modeled as an incompressible Stokes flow between solid particles randomly distributed at fixed locations. When the rigid skeleton occupies most of the volume and the characteristic pore size is much smaller than the characteristic length scale in the fluid flow driven by a pressure jump, the incompressible Darcy's equations are found to describe such porous medium flow[1]. Nonlinear drag between the fluid flow and the solid structures has been incorporated to account for the inertia effects at high Reynolds number. Brinkman suggested modifying Darcy's equations to incorporate the dissipation in the fluid phase via an effective fluid viscosity but did not provide a detailed derivation. When the fluid flow occupies most of the volume and the porous structures occupies less than 5% of the total volume, rigorous homogenization does give rise to the incompressible Brinkman equations with the effective viscosity of Brinkman fluid identical to the Stokesian fluid viscosity[1].

The motion of a spherical porous particle freely suspended in a Stokes flow has been investigated[2–5]. The surface tension, essential for a spherical (or nearly spherical) viscous drop under linear flows, is replaced by the rigidity of the interior skeleton that is sufficiently strong to maintain a spherical shape with permeability on the interface. With the rigid skeleton fully hydrated the drag coefficient and total force are computed as a function of the interior porosity in various flowing conditions such as a streaming flow, uniaxial extensional flow, and a planar shear flow. In addition the migration of a spherical porous drop in a planar shear flow or near a flat fluid interface has also been investigated[4].

A steady equilibrium of a nearly spherical viscous drop with surface tension can be found in the small-deformation theory[6]. For a slightly deformable porous drop the interior skeleton sustains the initial spherical shape that evolves under a linear flow. It is not clear if a deformable porous drop will evolve towards a stable steady equilibrium shape under general linear flows, and the main focus of our work is to formulate the fully hydrated skeleton inside the drop as a biphasic fluid drop immersed in a viscous Stokesian fluid.

Mathematical analyses on the behavior and properties of a fully hydrated poro-elastic or poro-viscous-elastic network focus on either the Biot system where the inertia of the poro-elastic or poro-visco-elastic skeleton is important[7,8], or a similar Darcy poroelastic fluid but without the friction between the fluid phase and the solid phase[9–11]. In this work we focus on regimes where the skeleton inertia is negligible and yet the skeleton undergoes elastic displacement, such as connective tissues or intracellular cytosols in many biological appli-

cations. Such a scenario has been considered without the interaction between an exterior fluid flow[9,12] When the porous structures are deformable and fully hydrated by a Stokesian viscous fluid, compressing the porous material will decrease the volume of the pore space, driving fluid out. Similarly, injecting fluid into a deformable porous material can expand the pore space, distorting the underlying skeleton. Multi-phase models have been derived to described the coupled dynamics between the deformable porous structures and the surrounding viscous fluid flow.

MacMinn *et al.* investigated the effects of nonlinear elasticity of the porous skeleton on the interior Darcy flow[12]. In the presence of an external pressure jump, MacMinn *et al.* focused on the coupling between the interior fluid flow and the deformation of the elastic porous structures and reported both small and large deformations of the poro-elastic structures using various elastic models. In particular they studied the one-dimensional dynamic evolution from an initial configuration towards a steady equilibrium.

While the pressure-driven Darcy flow inside a poroelastic skeleton is of great relevance in geophysics, biological poromechanical flows often involve the coupling between an exterior viscous fluid flow and an interior poroelastic flow, see work by Lai *et al.*[13]. In these models, the viscous dissipation in the fluid phase may be comparable to the pressure gradient, and this poromechanical coupling is further complicated by ion transport in the porous medium flow, see work by Pinsky *et al.*[14–16]. Cogan and Keener developed a two-phase flow model for cellular cytosol, with a dominant viscous dissipation of a deformable skeleton (that depends on the rate of strain) and no elastic energy (that depends on the strain)[17]. The dynamic coupling between mechanical and electrochemical effects of polyelectrolyte gels has been formulated by Mori *et al.*[18]. Focusing on the variational derivation of the governing equations in the mean-field framework, their dynamical model consists of many parameters that are related to the underlying microscopic physics and transport in the transition region around the domain boundary.

In addition to the complexity of structures and transport inside a deformable porous media, additional modeling issues arise at the interface between regions. Finding effective boundary conditions near the surface of such heterogeneous materials is a very difficult problem. This difficulty can be seen by the transition from a Darcy flow in the bulk region to a Brinkman flow in the transition region around the boundary between a porous medium and a viscous fluid flow. As a result, the standard techniques of homogenization break down close to the boundaries. To better understand the interface region, experiments and numerical simulations have been used to characterize velocity fields at different scales of the interfacial region between a fluid and a porous layer. For example, measurement techniques (such as particle image velocimetry, PIV) have provided velocity profiles and estimation of the size of the interfacial layer for granular and fibrous porous media[19]. Pore-scale numerical simulations also lead to local representations in the interfacial region.

When the thickness of the interfacial transition region is very small compared to the macroscopic length scale, Angot, Goyeau and Ochoa-Tapia's asymptotic analysis on the transition layer between a Stokes fluid and a Darcy-Brinkman fluid leads to an algebraic jump boundary conditions at a fictive dividing interface between the homogeneous fluid and porous regions[20]. Using the ratio of pore size to the macroscopic length scale as a small

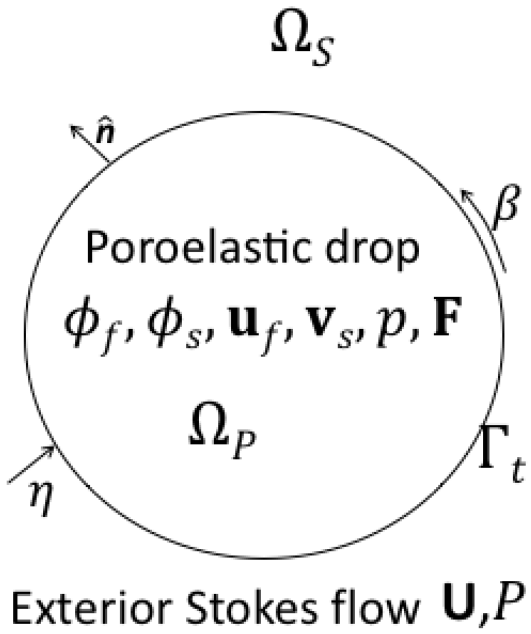

FIG. 1. Sketch of a poroelastic drop in Ω_P immersed in a Stokesian fluid in Ω_S. Inside the drop there is a fluid phase (subscript 'f') and a skeleton phase (subscript 's') which is bounded by the deformable interface Γ_t. $\hat{\mathbf{n}}$ is the outward normal, β is the slip coefficient, and η is the permeability on the interface.

parameter, the dominant jump conditions are found at the first order, and the generality of such asymptotic analysis allows them to make direct comparison with several pre-existing models such as the pioneering slip model by Beavers and Joseph[21]. It is worth mentioning that the approach adopted by Angot *et al.*[22–24] was suggested by Worster *et al.*[25,26], where the empirical formula for the jump boundary conditions is similar to those used and/or derived in many other works[27–37].

In this work we focus on the hydrodynamics of a poroelastic material enclosed in a drop suspended in a viscous Stokes flow under two flowing conditions: a uniform flow and an uniaxial extensional flow. We derive the boundary conditions on the drop by free energy dissipation principle. Using these boundary conditions, we investigate how a poroelastic drop deforms when it is immersed in a uniaxial extensional flow and a planar shear flow. The hydrodynamics of a viscous drop in these two flows has been extensively studied as paradigms in fluid mechanics and microfluidic engineering. Focusing on the small-deformation dynamics and steady equilibria, we calculate the flow pattern and examine how the boundary conditions and poroelasticity affects the flow in and around the drop.

II. FORMULATION

Our problem is to study the dynamics of a poroelastic drop immersed in a Stokesian fluid acted upon by an applied flow. Let Ω_P represent the region of the drop, Ω_S the region of the

exterior Stokes fluid, and Γ_t the interface between the poroelastic drop and the Stokesian fluid that evolves with time t, see Figure 1. Inside the poroelastic drop there are two phases: a skeleton phase (subscript 's') and a fluid phase (subscript 'f'). The skeleton phase is confined within Ω_P, while the fluid may permeate in or out of the boundary Γ_t. Cartesian coordinates centered at the initial drop center will be denoted by (x, y, z), and spherical coordinates by (r, θ, ϕ).

A. Two-phase flow model

We start by assuming that a soft poro-elastic drop is freely suspended in a Newtonian viscous fluid with the velocity $\mathbf{U}$ and pressure P satisfying the incompressible Stokes equations

$$\mu_e \nabla^2 \mathbf{U} - \nabla P \equiv \nabla \cdot (2\mu_e \mathbf{E}) - \nabla P = 0, \tag{1}$$

$$\nabla \cdot \mathbf{U} = 0, \tag{2}$$

where μ_e is the viscosity of the exterior fluid and $\mathbf{E} \equiv \left(\nabla \mathbf{U} + (\nabla \mathbf{U})^T\right)/2$ is the strain rate tensor of the exterior fluid. Inside the drop an elastic skeleton is fully hydrated, filled with the same viscous fluid as the outside. The mixture of the elastic skeleton and the interior viscous fluid is coarse-grained into a two-phase flow, with the skeleton phase of volume fraction ϕ_s the fluid phase of volume fraction ϕ_f, and $\phi_f + \phi_s = 1$. Conservation of fluid phase and skeleton phase inside the drop gives

$$\frac{\partial \phi_f}{\partial t} + \nabla \cdot (\phi_f \mathbf{u}_f) = 0, \tag{3}$$

$$\frac{\partial \phi_s}{\partial t} + \nabla \cdot (\phi_s \mathbf{u}_s) = 0, \tag{4}$$

with $\mathbf{u}_f$ the fluid velocity and $\mathbf{u}_s = d\mathbf{v}_s/dt$ the skeleton velocity, computed from taking the time derivative of the displacement field $\mathbf{v}_s$ of the skeleton. In addition, from Equations (3) and (4) we define an average local velocity $\mathbf{q} \equiv \phi_f \mathbf{u}_f + (1 - \phi_f)\, \mathbf{u}_s$ that is incompressible:

$$\nabla \cdot \mathbf{q} = \nabla \cdot (\phi_f \mathbf{u}_f + (1 - \phi_f)\, \mathbf{u}_s) = 0. \tag{5}$$

Denoting the stress tensor of the skeleton phase as σ_s and the strain rate tensor of the interior fluid phase as $\mathbf{e}_f$, the governing equations for the mixture of viscous fluid and poroelastic skeleton within the drop are

$$\nabla \cdot (\phi_f\, (2\mu_i \mathbf{e}_f)) - \phi_f \nabla p + \mathcal{F}^{s \to f} = 0, \tag{6}$$

$$\nabla \cdot (\phi_s \sigma_s) - \phi_s \nabla p + \mathcal{F}^{f \to s} = 0, \tag{7}$$

where $\mathbf{e}_f \equiv (1/2)\left(\nabla \mathbf{u}_f + (\nabla \mathbf{u}_f)^T\right)$ is the symmetric velocity gradient tensor for the interior fluid. Here μ_i is the effective viscosity of the fluid in the poroelastic drop. In general, $\mu_i \neq \mu_e$, but for small ϕ_s, they should be approximately equal[1]. The forces from the skeleton on the fluid are anti-forces to forces from the fluid on the skeleton: $\mathcal{F}^{s \to f} = -\mathcal{F}^{f \to s}$. Assuming

that the friction between the interior fluid and the elastic skeleton is dominant over other interaction forces, in this work these two forces take the following form

$$\mathcal{F}^{s\to f} = -\xi\phi_f\phi_s\left(\mathbf{u}_f - \mathbf{u}_s\right) = -\mathcal{F}^{s\to f}, \tag{8}$$

where ξ is the drag coefficient assumed to be constant.

The most general skeleton stress tensor σ_s consists of both a viscous stress σ_v (that depends on the gradient of the rate of strain $\mathbf{u}_s$) and an elastic stress σ_e (that depends on the gradient of the displacement $\mathbf{v}_s$ of the elastic skeleton): $\sigma_s = \sigma_v(\nabla\mathbf{u}_s) + \sigma_e(\nabla\mathbf{v}_s)$. The viscous stress of the skeleton depends on the rate of strain $\mathbf{u}_s$ as

$$\sigma_v \equiv \mu_s\left[\nabla\mathbf{u}_s + (\nabla\mathbf{u}_s)^T\right] - \tilde{\mu}_s\nabla\cdot\mathbf{u}_s, \tag{9}$$

where the compressible component on the righthand side is assumed to be negligible for small deformations. We adopt the Hencky elasticity and write the elastic stress as

$$\sigma_e(\nabla\mathbf{v}_s) \equiv \mathbf{\Lambda}\mathrm{tr}(\mathbf{H})\mathbf{I} + (\mathcal{M}-\mathbf{\Lambda})\mathbf{H},\ \ \mathbf{H} \equiv \frac{\mathbf{1}}{\mathbf{2}}\ln\left(\mathbf{F}\mathbf{F}^{\mathbf{T}}\right), \tag{10}$$

where the p-wave modulus $\mathcal{M} = K + \frac{4}{3}G$ and Lamé's first parameter $\mathbf{\Lambda} = K - \frac{2}{3}G$ are combinations of the bulk (K) and shear (G) moduli. Note that in general $\mathcal{M} > \mathbf{\Lambda}$ and the Poisson ratio of the elastic skeleton is $\nu \equiv \mathbf{\Lambda}/\left(\mathcal{M}+\mathbf{\Lambda}\right)$. The deformation gradient tensor $\mathbf{F}$ is defined as

$$\mathbf{F} = (\nabla\mathbf{X})^{-\mathbf{1}} = \left(\mathbf{I} - \nabla\mathbf{v_s}\right)^{-\mathbf{1}}. \tag{11}$$

When the strain of the poroelastic skeleton is small the volume fraction ϕ_f can be approximated as

$$\frac{\phi_f - \phi_0}{1-\phi_0} \approx \nabla\cdot\mathbf{v}_s \sim \epsilon \ll 1, \tag{12}$$

where ϕ_0 is the uniform fluid volume fraction distribution prior to the perturbation. In the small-strain limit, linear elasticity applies and we have

$$\sigma_e = \mathbf{\Lambda}\mathrm{tr}(\varepsilon)\mathbf{I} + (\mathcal{M}-\mathbf{\Lambda})\varepsilon,\ \ \varepsilon = \frac{1}{2}\left[\nabla\mathbf{v}_s + (\nabla\mathbf{v}_s)^T\right]. \tag{13}$$

In the following we focus on slightly deformable poroelastic structures with both an elastic stress and a viscous stress.

B. Boundary Conditions

The boundary conditions at the interface between two homogeneous phases are usually derived by enforcing the conservation of mass and continuity of stress across the interface. This will be done here but these conditions are not sufficient for our multiphase drop. The difficulty is because we are connecting a single phase region with a two-phase region and we are considering only on the macroscopic scale of the drop, i.e., the pore scale dynamics is coare-grained in the biphasic model. The principal of free energy dissipation will be used to derive the additional boundary conditions.

Ignoring the surface tension and assuming that the same viscous fluid is in both Ω_S and Ω_P, the "interface" Γ_t here is the boundary that encloses all the elastic skeleton in Ω_P. Defined as such, the boundary Γ_t moves with velocity v_Γ determined only by the skeleton phase of the interior since the fluid phase is permeable to the boundary. Thus, instead of the usual kinematic boundary condition where the time derivative of Γ_t is equal to the normal component of the fluid velocity evaluated on Γ_t, our first boundary condition is the kinematic condition for a permeable interface with a skeleton inside:

$$\mathbf{u}_s\Big|_{\Gamma_t} \cdot \hat{\mathbf{n}} = v_{\Gamma_t}. \tag{14}$$

Conservation of fluid mass at the interface Γ_t demands that the mass of fluid leaving the poroelastic drop in the normal direction from Ω_P balance the mass of fluid entering the region Ω_S. Since the fluids are incompressible and the same in both regions we find that,

$$(\mathbf{U} - \mathbf{u}_s)\Big|_{\Gamma_t} \cdot \hat{\mathbf{n}} = \phi_f \left(\mathbf{u}_f - \mathbf{u}_s\right)\Big|_{\Gamma_t} \cdot \hat{\mathbf{n}}. \tag{15}$$

Continuity of stress at the interface requires that the total stress of the Stokes flow side of the interface Γ_t be balanced by the total stress on the poroelastic side. The result is,

$$(-2\mu_e\mathbf{E} + P\mathbf{I} + \phi_f(2\mu_i\mathbf{e}_f) + \phi_s\sigma_s - p\mathbf{I})\Big|_{\Gamma_t} \cdot \hat{\mathbf{n}} = 0. \tag{16}$$

Equations (15)-(16) are not sufficient to find a unique solution to the problem.

In order to find the additional boundary conditions we begin by integrating the product of $\mathbf{U}$, $\mathbf{u}_f$ and $\mathbf{u}_s = d\mathbf{v}/dt$ with equations (1), (6), and (7), respectively, over the whole region $\Omega = \Omega_S + \Omega_P$. Use (2), (3), (4) and apply the divergence theorem to find:

$$\begin{aligned} 0 = &\int_{\Omega_S} \mathbf{U} \cdot \left[\nabla(2\mu_e\mathbf{E}) - \nabla P\right] d^3x \qquad (17)\\ &+ \int_{\Omega_P} \mathbf{u}_f \cdot \left[\nabla\left(\phi_f\left(2\mu_i\mathbf{e}_f\right)\right) - \phi_f\nabla p - \xi\phi_f\phi_s(\mathbf{u}_f - \mathbf{u}_s)\right] d^3x\\ &+ \int_{\Omega_P} \mathbf{u}_s \cdot \left[\nabla\cdot(\phi_s\sigma_s) - \phi_s\nabla p + \xi\phi_f\phi_s(\mathbf{u}_f - \mathbf{u}_s)\right] d^3x\\ &= \int_{\Gamma_t} -\mathbf{U}\cdot(2\mu_e\mathbf{E} - P\mathbf{I})\cdot\hat{\mathbf{n}}ds + \int_{\Gamma_t} \mathbf{u}_f\cdot\left(\phi_f\left(2\mu_i\mathbf{e}_f\right) - \phi_f p\mathbf{I}\right)\hat{\mathbf{n}}ds \qquad (18)\\ &+ \int_{\Gamma_t} \mathbf{u}_s\cdot(\phi_s\sigma_s - \phi_s p\mathbf{I})\hat{\mathbf{n}}ds - I_{\Omega_S} - I_{\Omega_P} - I_E, \end{aligned}$$

where

$$I_{\Omega_S} = \int_{\Omega_S} 2\mu_e\mathbf{E} : \nabla\mathbf{U}d^3x \tag{19}$$

$$I_{\Omega_P} = \int_{\Omega_P} \phi_f(2\mu_i\mathbf{e}_f) : \nabla\mathbf{u}_f + \xi\phi_f\phi_s\left\|\mathbf{u}_f - \mathbf{u}_s\right\|^2 d^3x + \int_{\Omega_P} \phi_s\sigma_v\left(\nabla\mathbf{u}_s\right) : \nabla\mathbf{u}_s d^3x, \tag{20}$$

$$I_E = \int_{\Omega_P} \phi_s\sigma_e\left(\nabla\mathbf{v}_s\right) : \nabla\mathbf{u}_s d^3x. \tag{21}$$

Here we have assumed that the surface integrals along the outer boundary of Ω_S are zero. This would be true for an applied flow where at this outer boundary the pressure balances the applied strain or for a flow where U tends to zero. After integration by parts, equation (18) shows that the sum of the two surface integrals on Γ_t and the two volume integrals I_{Ω_S} and I_{Ω_P} must equal to the volume integral I_E, which has been shown to be equal to the rate of change of an elastic free energy E_{elas}[18]:

$$I_E = \frac{dE_{elas}}{dt} = \int_{\Gamma_t} -\mathbf{U}\cdot(2\mu_e\mathbf{E} - P\mathbf{I})\cdot\hat{\mathbf{n}}ds + \int_{\Gamma_t}\mathbf{u}_f\cdot(\phi_f\,(2\mu_i\mathbf{e}_f) - \phi_f p\mathbf{I})\hat{\mathbf{n}}ds + \int_{\Gamma_t}\mathbf{u}_s\cdot(\phi_s\sigma_s - \phi_s p\mathbf{I})\hat{\mathbf{n}}ds - I_{\Omega_S} - I_{\Omega_P}, \tag{22}$$

where

$$E_{elas} = \int_{\Omega_P}\phi_s\mathcal{W}_{elas}(\mathbf{F})d^3x, \quad \text{with } \sigma_e(\mathbf{v}_s) = \frac{\partial\mathcal{W}_{elas}(\mathbf{F})}{\partial\mathbf{F}}\mathbf{F}^T, \tag{23}$$

where $\phi_s\mathcal{W}_{elas}$ is elastic energy per unit volume. Clearly the volume integrals are positive definite, thus one way to ensure $dE_{elas}/dt < 0$ is to choose boundary conditions such that the righthand side of Equation (22) is negative. We will use this observation to derive the boundary conditions.

Focusing on the surface integrals, denote the velocities relative to the skeleton velocity $\mathbf{u}_s$ with a bar as

$$\overline{\mathbf{U}} = \mathbf{U} - \mathbf{u}_s, \quad \overline{\mathbf{u}}_f = \phi_f(\mathbf{u}_f - \mathbf{u}_s), \tag{24}$$

the surface integrals in Equation (22) are thus recast as

$$\int_{\Gamma_t} -(\overline{\mathbf{U}} + \mathbf{u}_s)(2\mu_e\mathbf{E} - P\mathbf{I})\hat{\mathbf{n}} + \left(\frac{\overline{\mathbf{u}}_f}{\phi_f} + \mathbf{u}_s\right)(\phi_f(2\mu_i\mathbf{e}_f) - \phi_f p\mathbf{I})\hat{\mathbf{n}} + \mathbf{u}_s\,(\phi_s\sigma_s - \phi_s p\mathbf{I})\,\hat{\mathbf{n}}ds$$

$$= \int_{\Gamma_t}\mathbf{u}_s\cdot(-2\mu_e\mathbf{E} + P\mathbf{I} + \phi_f(2\mu_i\mathbf{e}_f) + \phi_s\sigma_s - p\mathbf{I})\hat{\mathbf{n}}ds + \tag{25}$$

$$\int_{\Gamma_t} -\overline{\mathbf{U}}\cdot(2\mu_e\mathbf{E} - P\mathbf{I})\hat{\mathbf{n}} + \overline{\mathbf{u}}_f\cdot(2\mu_i\mathbf{e}_f - p\mathbf{I})\hat{\mathbf{n}}ds. \tag{26}$$

Using the stress boundary condition Equation (16) we find that Equation (25) is zero. We note that when the drop interior is a single fluid phase ($\phi_f = 1$ and $\phi_s = 0$), the integral in Equation (26) vanishes because of velocity continuity $\overline{\mathbf{U}} = \overline{\mathbf{u}}_f$. In the more general cases $\phi_f \in (0,1)$ and the drop interior consists of two phases, more boundary conditions are to be derived from the integral in Equation (26).

To proceed further, we decompose $\overline{\mathbf{U}}$ and $\overline{\mathbf{u}}_f$ into the parallel (subscript '$\parallel$') and perpendicular (subscript '$\perp$') to the interface Γ_t as

$$\overline{\mathbf{U}} = \overline{\mathbf{U}}_\perp + \overline{\mathbf{U}}_\parallel, \quad \overline{\mathbf{u}}_f = \overline{\mathbf{u}}_{f\perp} + \overline{\mathbf{u}}_{f\parallel}. \tag{27}$$

Conservation of fluid mass from Equation (15) gives $\overline{\mathbf{U}}_\perp = \overline{\mathbf{u}}_{f\perp}$. To make the normal velocity component of (26) negative definite, a simple choice is to choose $\eta > 0$ such that

$$\overline{\mathbf{U}}_\perp = \eta\left\{\hat{\mathbf{n}}\cdot(2\mu_e\mathbf{E} - P\mathbf{I} - 2\mu_i\mathbf{e}_f + p\mathbf{I})\Big|_{\Gamma_t}\cdot\hat{\mathbf{n}}\right\}\hat{\mathbf{n}}. \tag{28}$$

For the tangential component, choices for $\overline{\mathbf{U}}_{\parallel}$ and $\overline{\mathbf{u}}_{f\parallel}$ must be made based on the condition that the integral in Equation (26) must be semi-negative definite. Onsager reciprocal principle dictates the following symmetric choices

$$\begin{pmatrix} \overline{\mathbf{u}}_{f\parallel} \\ \overline{\mathbf{U}}_{\parallel} \end{pmatrix} = \begin{pmatrix} \alpha & \beta \\ \beta & \gamma \end{pmatrix} \begin{pmatrix} \left(\mu_e \mathbf{E}|_{\Gamma_t} \cdot \hat{\mathbf{n}}\right)_{\parallel} \\ -\left(\mu_i \mathbf{e}_f|_{\Gamma_t} \cdot \hat{\mathbf{n}}\right)_{\parallel} \end{pmatrix}, \tag{29}$$

where α, β, and γ are chosen so that the contribution from the tangential components in Equation (26) is negative definite. Here we set $\alpha = \gamma = 0$ and $\beta > 0$ as a simple choice to ensure that Equation (22) is negative definite. We remark that when $\alpha = \gamma = 0$ and $\beta > 0$ the two boundary conditions for the tangential component of the relative velocities are simplified to

$$\overline{\mathbf{U}}_{\parallel} = \beta \left(\mu_e \mathbf{E}\Big|_{\Gamma_t} \cdot \hat{\mathbf{n}} \right)_{\parallel}, \tag{30}$$

$$\overline{\mathbf{u}}_{f\parallel} = -\beta \left(\mu_i \mathbf{e}_f\Big|_{\Gamma_t} \cdot \hat{\mathbf{n}} \right)_{\parallel}. \tag{31}$$

Furthermore, when the interior fluid is a Darcy fluid with a deformable skeleton the tangential component of the integrand in Equation (26) involves only the exterior velocity parallel to Γ_t. This is because when $\mu_i = 0$, $\mathbf{u}_{f\parallel}(-p\mathbf{I} \cdot \hat{\mathbf{n}})_{\parallel} = 0$, consequently there is one less tangential boundary condition for a Darcy drop. Interior slip in Equation (31) disappears naturally when $\mu_i = 0$.

In summary the boundary conditions for $\mathbf{U}$, $\mathbf{u}_f$ and $\mathbf{u}_s$ are given by (15), (16), (28), and (30). For future reference these can be collected here as:

$$\left[(\mathbf{U} - \mathbf{u}_s) - \phi_f \left(\mathbf{u}_f - \mathbf{u}_s \right) \right] \cdot \hat{\mathbf{n}} = 0, \tag{32}$$

$$\left(\mathbf{U} - \mathbf{u}_s \right)|_{\Gamma_t} \cdot \hat{\mathbf{n}} = \eta \hat{\mathbf{n}} \cdot \left[(2\mu_e \mathbf{E} - P\mathbf{I}) - (2\mu_i \mathbf{e}_f - p\mathbf{I}) \right] \cdot \hat{\mathbf{n}}, \tag{33}$$

$$\left(\mathbf{U} - \mathbf{u}_s \right)|_{\Gamma_t} \cdot \hat{\mathbf{t}} = \beta \hat{\mathbf{n}} \cdot \mu_e \mathbf{E}|_{\Gamma_t} \cdot \hat{\mathbf{t}}, \tag{34}$$

$$\phi_f \left(\mathbf{u}_f - \mathbf{u}_s \right)|_{\Gamma_t} \cdot \hat{\mathbf{t}} = -\beta \hat{\mathbf{n}} \cdot \mu_i \mathbf{e}_f|_{\Gamma_t} \cdot \hat{\mathbf{t}}, \tag{35}$$

$$\hat{\mathbf{n}} \cdot \left[(2\mu_e \mathbf{E} - P\mathbf{I}) - (\phi_s \sigma_s + \phi_f (2\mu_i \mathbf{e}_f) - p\mathbf{I}) \right] \cdot \hat{\mathbf{n}} = 0, \tag{36}$$

$$\hat{\mathbf{t}} \cdot \left[2\mu_e \mathbf{E} - (\phi_s \sigma_s + \phi_f \left(2\mu_i \mathbf{e}_f \right)) \right] \cdot \hat{\mathbf{n}} = 0, \tag{37}$$

where $\sigma_s = \sigma_e + \sigma_v$, $\eta > 0$ is a drag coefficient, and $\beta > 0$ is a slip coefficient. Equations (34)-(35) are consistent with the slip boundary condition derived by Angot *et al.*[20], and it is shown to be compatible with models previously derived for different configurations[20]. For a permeable moving boundary, the normal component of the total stress is from the fluid pressure and the shear component must vanish; this implies that both the normal and shear components of the effective stress must vanish. Equations (36)-(37) are for the stress balance at the boundary (more general than either permeable or impermeable boundaries) between a two-phase flow and a viscous Stokes flow. These are similar to the stress balance at the boundary between a polyelectrolyte gel and a Stokes flow in Mori *et al.*[18].

C. External linear flow field

We will apply the two-phase model to a slightly deformable porous drop in an axi-symmetric configuration with no dependence on the azimuthal angle ϕ. Recall that for axi-symmetric incompressible flows around a fluid drop there exists a stream function ψ_e for the exterior fluid flow

$$U_r = -\frac{1}{r^2 \sin\theta}\frac{\partial \psi_e}{\partial \theta},\ U_\theta = \frac{1}{r\sin\theta}\frac{\partial \psi_e}{\partial r},\ \ U_\phi = 0. \tag{38}$$

Here we will compare the flow around a viscous drop and a Darcy drop in either a planar shear flow or a uniaxial extensional flow. For a uniaxial extensional flow the far-field fluid velocity is

$$\mathbf{U} \to -G\,(x, y, -2z)\ \text{ as } r \to \infty, \tag{39}$$

where G is the extension rate. For a planar shear flow the far-field fluid velocity is

$$\mathbf{U} \to G(y, 0, 0) \text{ as } r \to \infty, \tag{40}$$

where now G is the shear rate of the background planar shear flow.

D. Non-dimensionalization

In our two-phase flow model the pore size is assumed to be much smaller than the drop size l_0, which is used to scale length in the nondimensionalization. Assume that over the length scale of l_0, there is a characteristic velocity U_0. For the two flows we will consider, we can select $U_0 = l_0 G$. In this work we will focus on the Darcy flow regime where $\mathcal{M} \gg \mu_i U_0/l_0$ and $\xi U_0 l_0/\mathcal{M} \sim \mathcal{O}(1)$, and both the elastic and friction forces dominate the viscous stress in equation (6). Thus the pressure is scaled by $\mathcal{M}$ and the dimensionless parameters are $\bar{\xi} = \xi U_0 l_0/\mathcal{M}$, $\bar{\Lambda} = \Lambda/\mathcal{M}$, $\bar{\alpha}_e = \mu_e U_0/\mathcal{M} l_0$, $\bar{\alpha}_v = \mu_s U_0/\mathcal{M} l_0$, slip coefficient $\bar{\beta} = \beta\mu_e/l_0 = \bar{\alpha}_e \beta \mathcal{M}/U_0$, and permeability $\bar{\eta} = \eta\mathcal{M}/U_0$. For the Darcy-Stokes system, the dimensionless equations are in their appropriate regions (and dropping the bar)

$$\alpha_e \nabla^2 \mathbf{U} - \nabla P = 0, \tag{41}$$

$$\nabla \cdot \mathbf{U} = 0, \tag{42}$$

$$-\phi_f \nabla p - \xi \phi_f \phi_s \left(\mathbf{u}_f - \mathbf{u}_s\right) = 0, \tag{43}$$

$$\nabla \cdot \left(\phi_s \left(\sigma_e + \alpha_v \sigma_v\right)\right) - \phi_s \nabla p + \xi \phi_s \phi_f \left(\mathbf{u}_f - \mathbf{u}_s\right) = 0, \tag{44}$$

$$\frac{\partial \phi_f}{\partial t} + \nabla \cdot \left(\phi_f \mathbf{u}_f\right) = 0, \tag{45}$$

$$\phi_f + \phi_s = 1, \quad \nabla \cdot \left(\phi_f \mathbf{u}_f + \phi_s \mathbf{u}_s\right) = 0. \tag{46}$$

The corresponding dimensionless boundary conditions on the interface Γ_t are

$$[(\mathbf{U}-\mathbf{u}_s)-\phi_f(\mathbf{u}_f-\mathbf{u}_s)]\cdot\hat{\mathbf{n}}=0, \tag{47}$$

$$(\mathbf{U}-\mathbf{u}_s)|_{\Gamma_t}\cdot\hat{\mathbf{n}}=\eta\hat{\mathbf{n}}\cdot[(2\alpha_e\mathbf{E}-P\mathbf{I})-(-p\mathbf{I})]\cdot\hat{\mathbf{n}}, \tag{48}$$

$$(\mathbf{U}-\mathbf{u}_s)|_{\Gamma_t}\cdot\hat{\mathbf{t}}=\beta\hat{\mathbf{n}}\cdot\mathbf{E}|_{\Gamma_t}\cdot\hat{\mathbf{t}}, \tag{49}$$

$$\hat{\mathbf{n}}\cdot[(2\alpha_e\mathbf{E}-P\mathbf{I})-(\phi_s(\sigma_e+\alpha_v\sigma_v)-p\mathbf{I})]\cdot\hat{\mathbf{n}}=0, \tag{50}$$

$$\hat{\mathbf{t}}\cdot[2\alpha_e\mathbf{E}-(\phi_s(\sigma_e+\alpha_v\sigma_v))]\cdot\hat{\mathbf{n}}=0. \tag{51}$$

E. Slip, permeability and surface tension at the boundary

The slip at the boundary between a Stokesian fluid and a Darcy medium arises from the uneven boundary (characterized by an average pore size a_0) that the viscous fluid flow has to go around. It is experimentally measured[21] to be of the order of the characteristic pore size divided by the viscosity of the external fluid: $\beta\sim a_0/\mu_e$. Thus the dimensionless slip coefficient $\bar{\beta}=a_0/l_0\ll 1$ because the ratio of the average pore size to the size of the drop is assumed to be small at the preset of the coarse-grained formulation. The interfacial permeability η is found to be of the same order as β by Haber and Mauri[38]. For the following results we vary η and β over a wide range to elucidate their effects on the small deformation of a poroelastic drop in linear flows. Large slip coefficient β at the Stokes-Darcy boundary is possible by coating the skeleton with special polymers[39]. Thus a wide range of β (and η) corresponds to a poroelastic skeleton treated chemically.

The surface tension is negligible at the boundary between a viscous Stokeian fluid and a Darcy medium. A viscous drop in linear flows (such as a planar shear flow and a uniaxial extensional flow) relies on a strong surface tension (small capillary number) to stay nearly spherical. The dynamic evolution from a spherical to a slightly deformed shape is governed by a exponential asymptote to equilibrium for any value of the viscosity ratio, which is the only physical parameter for a slightly-deformable viscous drop in linear flows (equation (8.81) in §8.3.C of Leal[6].) For a poroelastic drop, large bending moduli keep the drop shape close to spherical under linear flows. In this work we neglect the surface tension and focus on the Darcy regime, where a deformable Darcy drop is freely suspended in (1) a uniaxial extensional flow and (2) a planar shear flow. We focus on the physical regime where the elastic skeleton deforms slightly to contribute to the shape deviation of the drop from a sphere.

In such small-deformation limit the volume fraction of the elastic skeleton deviates very little from the original distribution. To elucidate the salient features of slip and permeability effects on the hydrodynamics of a soft poroelastic drop, we conduct a small-deformation analysis on a poroelastic drop of (nearly) an initially uniform porosity ϕ_0, and the nearly spherical drop shape is supported by a skeleton of large bending stiffness. The effects of non-uniform volume fraction (porosity) on the dynamics of an elastic poroelastic skeleton in one-dimension is the main focus of the work by MacMinn *et al.*[12]. It is a non-trivial extension to incorporate the non-uniform porosity into the small-deformation analysis. Based on results from MacMinn *et al.*[12] we expect to rely on numerical computations as analytical

solutions may not be readily available for a system of boundary value problems with variable coefficients.

Finally we remark that in the limit of infinitely large network elastic moduli $\mathcal{M} \approx \Lambda \gg 1$, the network becomes rigid (non-deformable) and both the displacement and the rate of strain vanish. Consequently less boundary conditions are needed in this non-deformable limit, and early works have focused on the balance of normal stress and continuity of the normal component of the fluid velocity[5,30,40].

III. SMALL-DEFORMATION OF A POROELASTIC DARCY DROP

In this section we investigate the flow around a poroelastic drop with large bending moduli such that the elastic skeleton (and hence the drop interface) undergoes small deformation from the initial spherical shape. On the interface Γ_t

$$r = 1 + \delta r(t, \theta, \phi) = 1 + \mathbf{v}_s \cdot \hat{\mathbf{r}}, \quad |\delta r| = |\mathbf{v}_s \cdot \hat{\mathbf{r}}| \ll 1. \tag{52}$$

In the small-deformation limit, the linear Stokes equations for the exterior fluid are coupled to the interior poroelastic fluid via the boundary conditions evaluated at the unperturbed spherical interface. This way the governing equations are a linear system that can still be solved using the separation of variables. In our small-deformation approximation, the volume fractions ϕ_f and ϕ_s are assumed to be initially homogeneous. The deviation from the initial homogeneous distribution is related to the divergence of the displacement field in Equation 12, and the rate of strain field

$$\mathbf{u}_s = \frac{d\mathbf{v}_s}{dt} = \frac{\partial \mathbf{v}_s}{\partial t} + \mathbf{u}_s \cdot \nabla \mathbf{v}_s \approx \frac{\partial \mathbf{v}_s}{\partial t}. \tag{53}$$

In the small-deformation framework the volume fraction perturbation is approximated by the divergence of the strain in Equation (12).

We solve Equations (41)-(45) linearized around the spherical shape. The linearized Darcy equations and the governing equations for stress balance in the solid phase are

$$-\phi_0 \nabla p - \xi \phi_0 (1 - \phi_0) \left(\mathbf{u}_f - \frac{\partial \mathbf{v}_s}{\partial t} \right) = 0, \tag{54}$$

$$\nabla \cdot \left((1 - \phi_0) \left(\sigma_e(\mathbf{v}_s) + \alpha_v \sigma_v(\mathbf{u}_s) \right) \right) - \nabla p = 0, \tag{55}$$

$$\nabla \cdot (\phi_0 \mathbf{u}_f + (1 - \phi_0)\mathbf{u}_s) = 0. \tag{56}$$

The general solution for the above linear equations take the following form

$$\begin{pmatrix} \mathbf{u}_f \\ \mathbf{v}_s \\ p \end{pmatrix} = \begin{pmatrix} \widehat{\mathbf{u}}_f \\ \widehat{\mathbf{v}}_s \\ \widehat{p} \end{pmatrix} + e^{\omega t} \begin{pmatrix} \mathbf{u}_{f,1} \\ \mathbf{v}_{s,1} \\ p_1 \end{pmatrix}, \tag{57}$$

where the hat symbol $\widehat{\cdot}$ denotes the steady equilibrium solution, and the subscripts "1" denotes the exponential components that vary with time at an exponential rate ω. In the following we will solve for both the steady equilibrium and the eigenvalue ω. Note that in the small-deformation limit $\mathbf{u}_s \sim \partial \mathbf{v}_s / \partial t = \omega e^{\omega t} \mathbf{v}_{s,1}$.

A. Steady Equilibrium

Within the small-deformation regime, a viscous drop with a large surface tension (small capillary number) reaches a steady shape under linear flows. Similarly for a nearly spherical poroelastic drop with a large network rigidity, we assume that it reaches a steady shape under linear flows. At steady equilibrium the normal component of the skeleton velocity $\mathbf{u}_s$ evaluated at the steady drop interface is zero.

The tangential components of the network velocity, on the other hand, depends on the exterior flow condition: Under a uniaxial extensional flow the tangential network velocity is zero at steady equilibrium, while under a planar shear flow the tangential network velocity is a rigid-body rotation due to the rotational component of the far-field shear flow. For the uniaxial extensional flow, the viscous dissipation of the network phase is zero at the steady equilibrium because $\mathbf{u}_s = d\mathbf{v}_s/dt = 0$. Thus the steady equilibrium solution does not depend on the network viscosity μ_s. For the linear shear flow, the network rotates due to the vorticity in the shear flow. This network rotation is a rigid-body rotation that does not cause any viscous dissipation. Thus we also do not expect the equilibrium solution to depend on μ_s for the shear flow case.

B. Uniaxial extensional flow

First we identify the steady equilibrium solution for a Darcy drop under a uniaxial extensional flow specified by Equation (39). At steady equilibrium, the general solutions for the drop interior take the form

$$\widehat{p} = -\frac{21}{10}(1-\phi_0)(1-\Lambda)d_1 r^2\left(1+3\cos(2\theta)\right), \tag{58}$$

$$\widehat{\mathbf{v}}_s \cdot \hat{\mathbf{r}} = \left(-\frac{3(5-2\Lambda)}{25}d_1 r^3 - d_2 r - \frac{2\Lambda}{7+3\Lambda}d_3 r^3\right)\left(1+3\cos(2\theta)\right), \tag{59}$$

$$\widehat{\mathbf{v}}_s \cdot \hat{\theta} = \left(\frac{3(6-\Lambda)}{25}d_1 r^3 + d_2 r + \frac{1}{3}d_3 r^3\right)\sin(2\theta), \tag{60}$$

and $\widehat{\mathbf{u}}_s = 0$ in the case of a uniaxial extensional flow. Here $\hat{\mathbf{r}}$ and $\hat{\theta}$ are unit vectors in the r and θ directions. The solution for the exterior Stokes flow is

$$\widehat{\psi}_e = \left(r^3 - \frac{A_1}{2} - \frac{A_2}{2r^2}\right)\cos\theta\sin^2\theta, \tag{61}$$

$$\widehat{P}_e = -\frac{\alpha_e}{2r^3}A_1\left(1+3\cos(2\theta)\right), \tag{62}$$

where ψ_e is the stream function and P_e is the pressure for the external fluid. Altogether there are five coefficients (A_1, A_2, d_1, d_2, d_3) to be determined by the five boundary conditions in Equations (47)-(51). We focus on parameter combinations that pertain to the small-deformation assumption. The expression for the five coefficients are given in Appendix A.

Figure 2 shows equilibrium radial displacement evaluated at the unperturbed radius $r = 1$ and its dependence on the interfacial slip β for different values of permeability η with

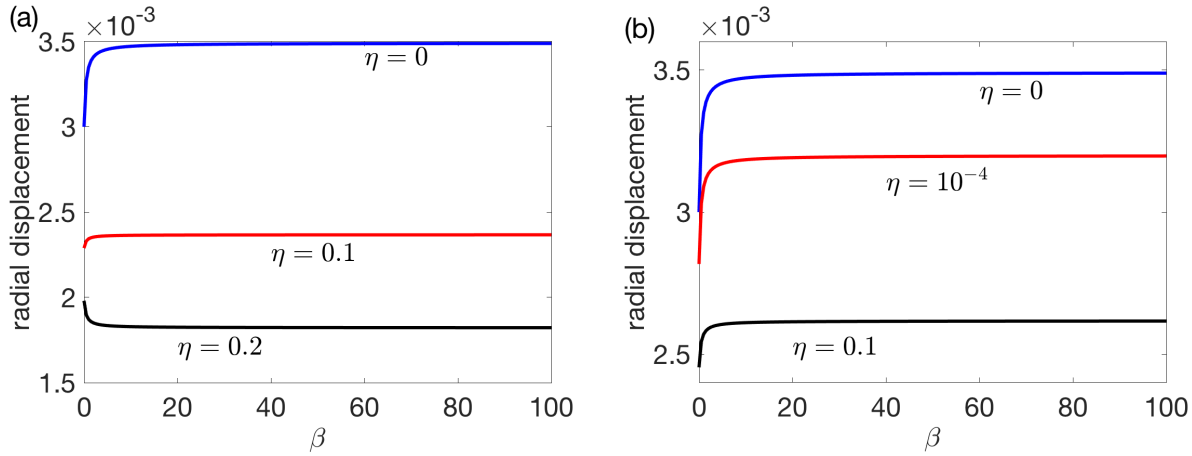

FIG. 2. Radial displacement $(\widehat{\mathbf{v}}_s \cdot \hat{\mathbf{r}})$ evaluated at $r = 1$ with $\Lambda = 1/3$, and $\phi_0 = 0.5$. (a) $\xi = 10^{-5}$. (b) $\xi = 10^{-1}$.

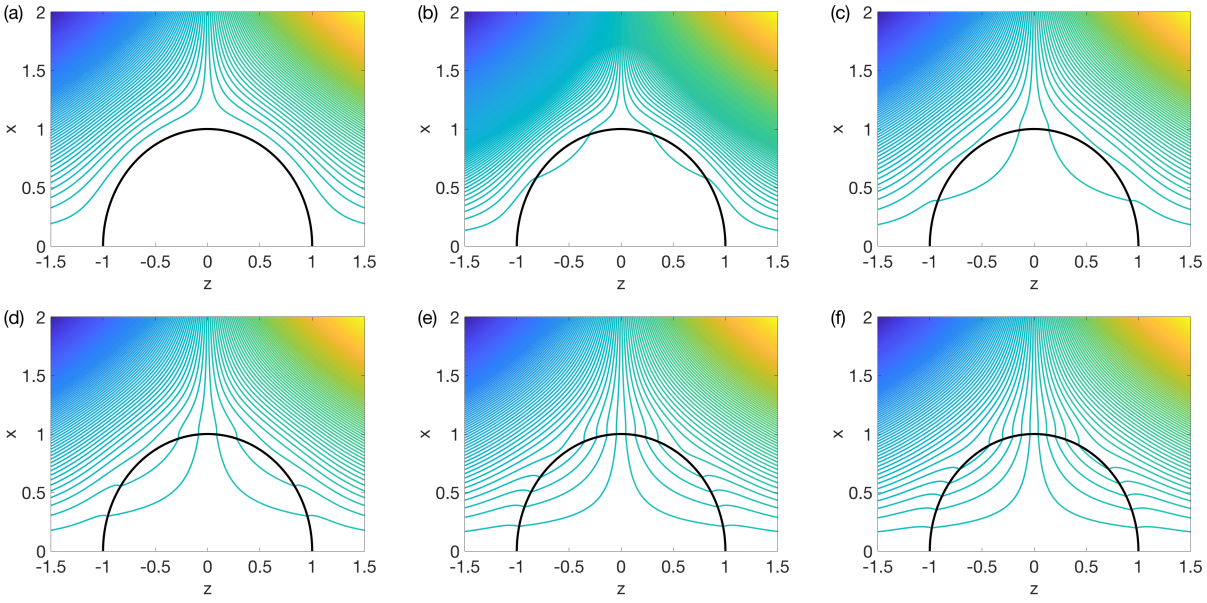

FIG. 3. Effect of permeability on the streamlines with $\Lambda = 1/3$, $\xi = 10^{-4}$ and $\beta = 0$. (a) $\eta = 0$, (b) $\eta = 0.01$, (c) $\eta = 0.05$, (d) $\eta = 0.1$, (e) $\eta = 0.5$, and (f) $\eta = 1$.

$\Lambda = 1/3$, and $\phi_0 = 0.5$. The drag coefficient $\xi = 10^{-5}$ for panel (a) and $\xi = 10^{-1}$ for panel (b). For these parameter values, the radial displacement appears to only weakly depend on ξ. Note how the displacement asymptotes to an equilibrium value with increasing β. Note also how increasing the permeability η decreases the displacement.

Figures 3 show the effects of the permeability on the streamlines at equilibrium with $\Lambda = 1/3$, $\xi = 10^{-4}$ and $\beta = 0$. As the permeability increases with no interfacial slip $\beta = 0$, more flow goes through the slightly deformed poroelastic drop under the uniaxial extensional flow. The streamlines in Figure 3(a) (no permeability and no interfacial slip, $\eta = \beta = 0$) are similar to those for a viscous drop under an extensional flow that goes around

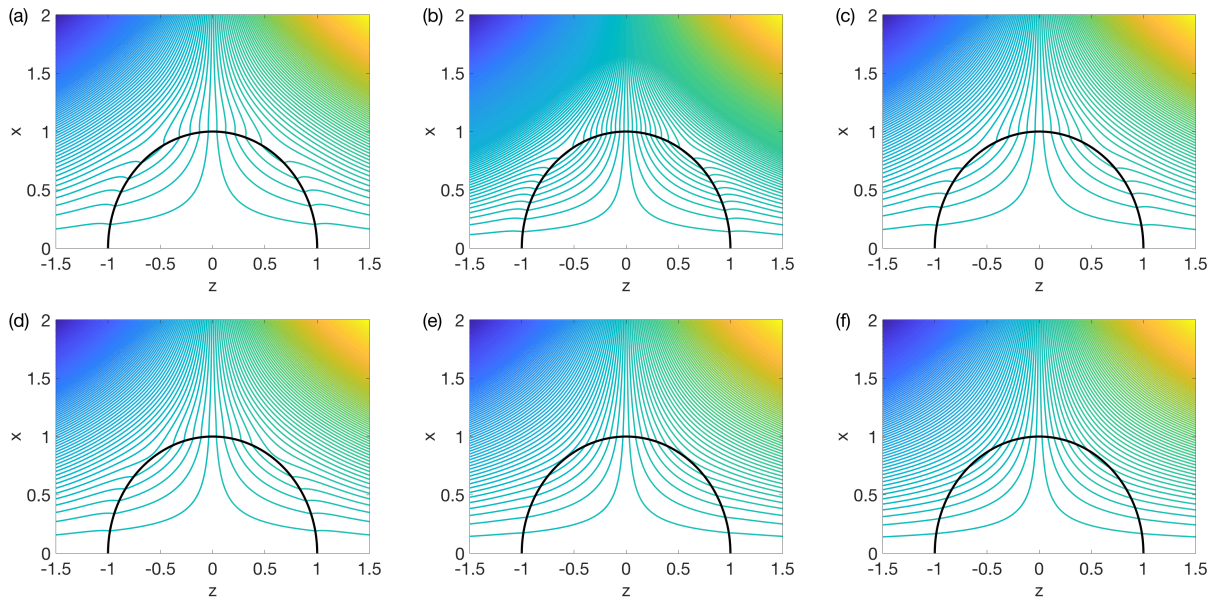

FIG. 4. Effect of interfacial slip on the streamlines with $\Lambda = 1/3$, $\xi = 10^{-4}$ and $\eta = 0.75$. (a) $\beta = 0$, (b) $\beta = 0.01$, (c) $\beta = 0.05$, (d) $\beta = 0.1$, (e) $\beta = 0.5$, and (f) $\beta = 1$.

the drop interface. As the permeability increases with $\beta = 0$, more flow goes through the drop interface as shown in the subsequent panels. At steady equilibrium under a uniaxial extensional flow, the displacement field velocity is zero and consequently the exterior flow goes through the drop surface along the inward normal direction. The interior flow, on the other hand, has a similar spatial pattern. In addition, we observe that the fluid flow can be discontinuous across the drop interface as expected from Equation (48).

Figure 4 shows the effects of the interfacial slip on the streamlines at equilibrium with $\Lambda = 1/3$, $\xi = 10^{-4}$ and $\eta = 0.75$. As the interfacial slip increases from $\beta = 0$ to $\beta = 1$, the discontinuity in the tangential flow decreases and the uniaxial extensional flow goes through the drop interface. There are less variations in the streamlines as β increases, consistent with the changes in the displacement field with increasing β shown in Figure 2.

Figure (5) shows the inflow in the first quadrant defined as

$$\text{inflow in first quadrant} = \frac{1}{2}\int_0^{2\pi}\int_0^{\pi/2} |\mathbf{U}|_{\Gamma_t} \cdot \hat{\mathbf{r}}| \sin\theta d\theta d\phi, \tag{63}$$

where the integral without the absolute sign would vanish due to symmetry of the perturbation, and hence the combination of factor $1/2$ and the absolute value sign gives the net inflow, which is exactly equal to the out-flow in the first quadrant. We observe that the net inflow increases with both slip and permeability.

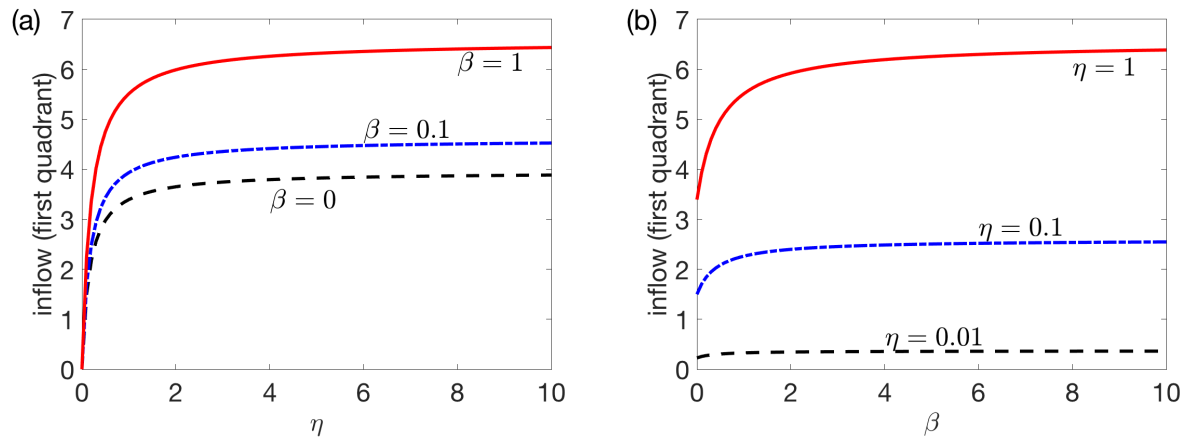

FIG. 5. Inflow as a function of η (panel (a)) and β (panel (b)). $\Lambda = 1/3$ and $\xi = 10^{-4}$.

C. Planar shear flow

For a poroelastic drop in a planar shear flow the interior equilibrium solution takes the form

$$\widehat{p} = \frac{1}{2} d_1 r^2 \sin^2\theta \sin(2\phi), \tag{64}$$

$$\widehat{\mathbf{v}}_s \cdot \hat{\mathbf{r}} = \left(\frac{1}{7(1-\Lambda)(1-\phi_0)} d_1 r^3 + d_3 r + \frac{2\Lambda}{7+3\Lambda} d_4 r^3 \right) \sin^2\theta \sin(2\phi), \tag{65}$$

$$\widehat{\mathbf{v}}_s \cdot \hat{\theta} = \left(\frac{5}{21(1-\Lambda)(1-\phi_0)} d_1 r^3 + d_3 r + \frac{1}{3} d_4 r^3 \right) \sin\theta \cos\theta \sin(2\phi), \tag{66}$$

$$\widehat{\mathbf{v}}_s \cdot \hat{\phi} = \left(-\frac{r}{2} t + \left(\frac{5}{21(1-\Lambda)(1-\phi_0)} d_1 r^3 + d_3 r + \frac{1}{3} d_4 r^3 \right) \cos(2\phi) \right) \sin\theta. \tag{67}$$

$\hat{\mathbf{r}}$, $\hat{\theta}$ and $\hat{\phi}$ are the unit vectors in the r, θ, and ϕ directions, respectively. The term $\frac{-r}{2}t$ in the ϕ-component of $\widehat{\mathbf{v}}_s$ (Equation (67)) is the rotation of the deformable elastic network induced by the external planar shear flow under the small-deformation framework. This rotation is also present in a viscous drop under a planar shear flow. The corresponding network rotation velocity at equilibrium is $\widehat{\mathbf{u}}_s = -r/2 \sin\theta \hat{\phi}$, which is a rigid body rotation and does not cause any viscous dissipation.

The exterior Stokes flow takes the form

$$\widehat{\mathbf{U}} \cdot \hat{\mathbf{r}} = \frac{1}{20 r^4} \left(6C_3 + 5C_1 r^2 + 10 r^5 \right) \sin^2\theta \sin(2\phi), \tag{68}$$

$$\widehat{\mathbf{U}} \cdot \hat{\theta} = \frac{1}{20 r^4} \left(-2C_3 + 5r^5 \right) \sin(2\theta) \sin(2\phi), \tag{69}$$

$$\widehat{\mathbf{U}} \cdot \hat{\phi} = -\frac{1}{10 r^4} \left(5(2C_4 r^2 + r^5) + (2C_3 - 5r^5) \cos(2\phi) \right) \sin\theta, \tag{70}$$

$$\widehat{P} = \frac{\alpha_e}{2r^3} C_1 \sin^2\theta \sin(2\phi). \tag{71}$$

The coefficient C_4 is zero, as expected from the small deformation analysis of a viscous drop in a planar shear flow. Altogether there are five coefficients $(d_1, d_3, d_4, C_1, C_3)$ to be

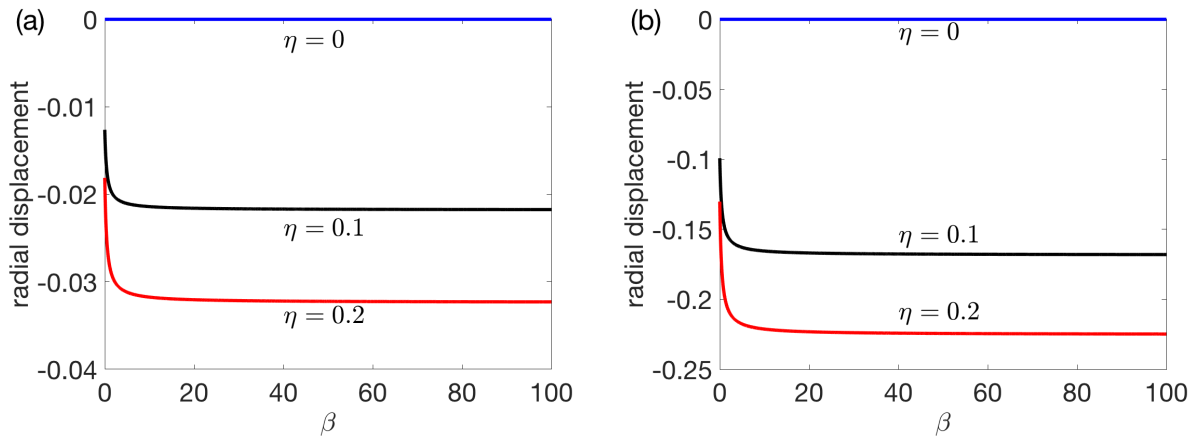

FIG. 6. Radial displacement $(\widehat{\mathbf{v}}_s \cdot \hat{\mathbf{r}})$ evaluated at $r = 1$ with $\Lambda = 1/3$, and $\phi_0 = 0.5$. (a) $\xi = 10^{-5}$. (b) $\xi = 10^{-4}$.

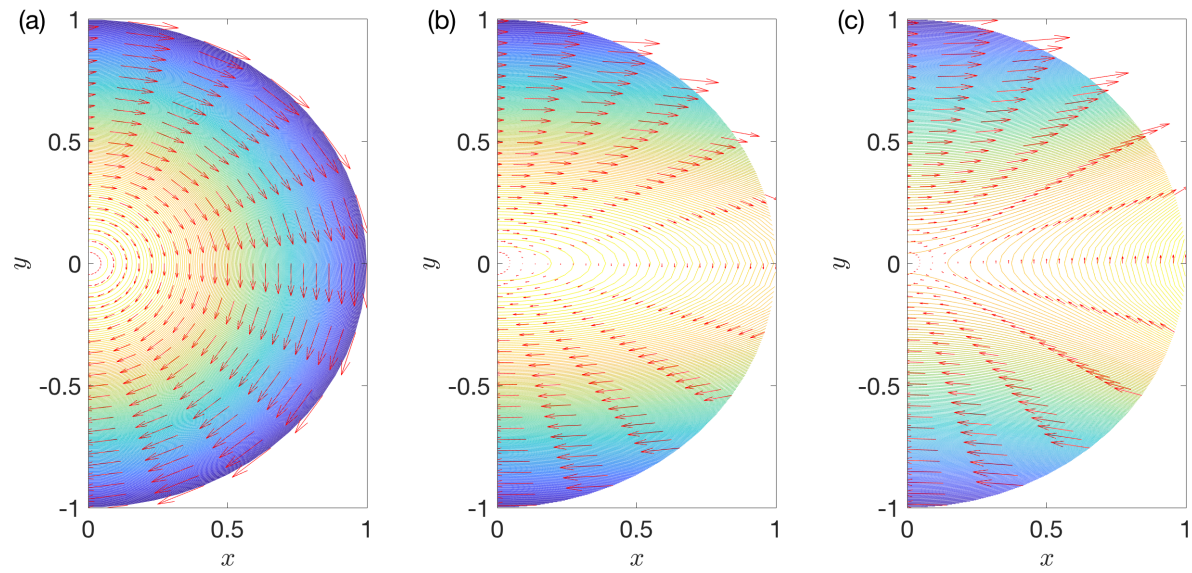

FIG. 7. Flow inside a poroelastic drop in a planar shear flow with $\phi_0 = 0.5$ and $\xi = 10^{-4}$. (a) $\eta = 0$ and $\beta = 0$, (b) $\eta = 100$ and $\beta = 0$, and (c) $\eta = 100$ and $\beta = 100$.

determined from seven boundary conditions (Equations (47)-(51) in three dimensions), from which there are only five linearly independent equations (similar to the small-deformation analysis of a viscous drop). The coefficients are listed in Appendix B.

Figure 6 shows radial displacement evaluated at the unperturbed drop surface ($r = 1$) as a function of slip for different values of permeability η with $\Lambda = 1/3$, and $\phi_0 = 0.5$. $\xi = 10^{-5}$ for panel (a) and $\xi = 10^{-4}$ for panel (b). As in the previous extensional flow case, the displacement asymptotes to a constant value with increasing β and decreases with increasing η. Here we do see a stronger effect of the drag coefficient ξ.

Figure 7 shows the interior flow of a poroelastic drop in the $x - y$ plane with $(\eta, \beta) =$

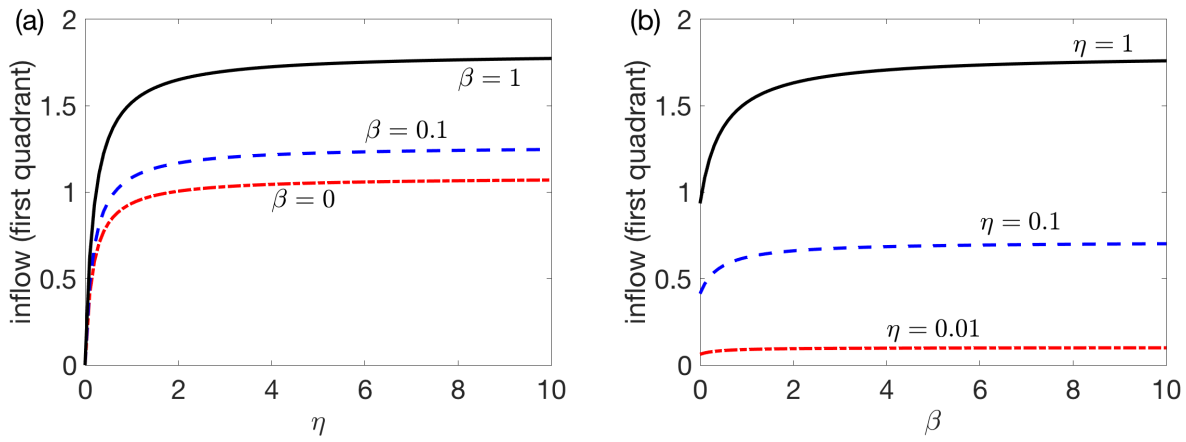

FIG. 8. Inflow as a function of η (panel (a)) and β (panel (b)). $\Lambda = 1/3$ and $\xi = 10^{-4}$.

$(0, 0)$ for panel (a), $(\eta, \beta) = (100, 0)$ for panel (b), and $(\eta, \beta) = (100, 100)$ for panel (c). The far-field flow is $\mathbf{U} = y\hat{\mathbf{x}}$. At steady equilibrium the z-component of the interior flow (Equations (64)-(67)) vanishes and we plot the interior flow in the $x - y$ plane. For $(\eta, \beta) = (0, 0)$ (panel (a)) the interior flow is a simple rotation. When the interface is permeable (non-zero permeability) the interior flow is almost like the planar shear flow outside except around the x-axis where the rotation dominates around the equator. In addition the interior flow develops a different pattern that depends on the interfacial slip β. When $\beta = 100$ (panel (c)) the interior flow develops a recirculation around the y-axis, which is not found for $\beta = 0$ (panel (b)). Figure (8) shows the inflow in the first quadrant defined in Equation (63) for the planar shear flow case. We observe that the net inflow increases with both slip and permeability, similar to the case of uniaxial extensional flow.

D. Linear Dynamics

Similar to the case of a slightly deformable viscous drop in linear flows, the steady equilibrium solution for a slightly deformed poroelastic drop is obtained from solving a non-homogeneous equation. For a viscous drop in linear flows, the kinematic boundary condition gives rise to a first-order differential equation for the deformation amplitude that decays exponentially to the steady equilibrium. The exponential decay rate depends only on the viscosity ratio between internal and external viscous fluids.

This is not the case for a poroelastic drop where the kinematic boundary condition is not sufficient for determining the linear dynamics characterized by a linear growth rate ω. Instead, because of the network viscous dissipation, the homogeneous component of the general solution in Equation (57) amounts to a nonlinear eigenvalue problem for ω.

The time dependent linear solutions for a poroelastic drop in a uniaxial extensional flow and a planar shear flow are given in Appendix C and Appendix D, respectively. The two functions g_1 and g_2 in Equations (C4)-(C5) for the uniaxial flow are identical to the g_1 and g_2 in Equations (D5)-(D6) for the planar shear flow. Both g_1 and g_2 are power series that

depend on ω:

$$g_1(r) = r^5 + \frac{2\bar{\omega}}{99}r^7 + \frac{5\bar{\omega}^2}{20592}r^9 + \frac{\bar{\omega}^3}{514800}r^{11} + \cdots, \tag{72}$$

$$g_2(r) = \frac{28}{\bar{\omega}}r^3 - \frac{1}{3}r^5 - \frac{\bar{\omega}}{198}r^7 - \frac{\bar{\omega}^2}{20592}r^9 - \frac{\bar{\omega}^3}{3088800}r^{11} + \cdots, \tag{73}$$

where

$$\bar{\omega} \equiv \frac{\omega\xi}{(1+\omega\alpha_v)\phi_0}. \tag{74}$$

For the uniaxial extensional flow case, the coefficients (a_1, a_2) in Equations (C6)-(C7) can be expressed in terms of $(\alpha_1, \alpha_3, \alpha_5)$. For the planar shear flow case, the coefficients (c_1, c_3) in Equations (D7)-(D10) can be eliminated as well. For both uniaxial and shear flow, the the resultant system of linear equations for $(\alpha_1, \alpha_3, \alpha_5)$ are thus a nonlinear eigenvalue problem for ω:

$$\mathbf{A}\begin{pmatrix}\alpha_1\\ \alpha_3\\ \alpha_5\end{pmatrix} = \omega\mathbf{B}(\omega)\begin{pmatrix}\alpha_1\\ \alpha_3\\ \alpha_5\end{pmatrix}. \tag{75}$$

Solutions of Equation (75) for ω describe the linear dynamics of a poroelastic drop in the small-deformation limit. Identical matrixes $\mathbf{A}$ and $\mathbf{B}$ are obtained for both the uniaxial extensional flow and the planar shear flow: This is consistent with the small-deformation dynamics of a viscous drop in linear flows. This means that the same eigenvalues are expected for both the uniaxial extensional flow and the planar shear flow.

The characteristic equations in matrix form are provided in supplementary material[41]. In the limit of $1 \ll \alpha_v|\omega|$, the eigenvalues ω can be calculated from a generalized eigenvalue problem and equation (75) can be reduced to a linear generalized eigenvalue problem as

$$\frac{\omega\xi}{(1+\omega\alpha_v)\phi_0} \to \frac{\xi}{\alpha_v\phi_0} \text{ as } \alpha_v|\omega| \gg 1, \quad \mathbf{A}\begin{pmatrix}\alpha_1\\ \alpha_3\\ \alpha_5\end{pmatrix} \approx \omega\mathbf{B_0}\begin{pmatrix}\alpha_1\\ \alpha_3\\ \alpha_5\end{pmatrix}, \tag{76}$$

with $\mathbf{B}_0$ independent of ω. The entries of matrix $\mathbf{B}_0$ are also provided in supplementary material[41]. It is worth noting that while there are three eigenvalues from Equation (76) (as opposed to one eigenvalue for the slightly-deformable viscous drop), the nonlinear eigenvalue system in Equation (75) may in general admit more than three eigenvalues.

Figures (9) show the first three eigenvalues from solving the full nonlinear eigenvalue problem in Equation (75) (solid curves) and the approximate linear eigenvalue problem in Equation (76) (dash-dotted curves) for three cases with different combination of β and η. For all these results, sufficient terms in the power series for g_1 and g_2 are used to guarantee convergence in finding the eigenvalue ω.

In general we find very good agreement in the first two eigenvalues between the full (solid lines) and approximated (dash-dotted lines) eigenvalue problem for volume fraction $0.1 \lessapprox \phi_0$. For $\phi_0 < 0.1$, panel (c) shows that complex eigenvalues (a complex conjugate pair with a negative real part) are found from Equation (76) while eigenvalues remain real

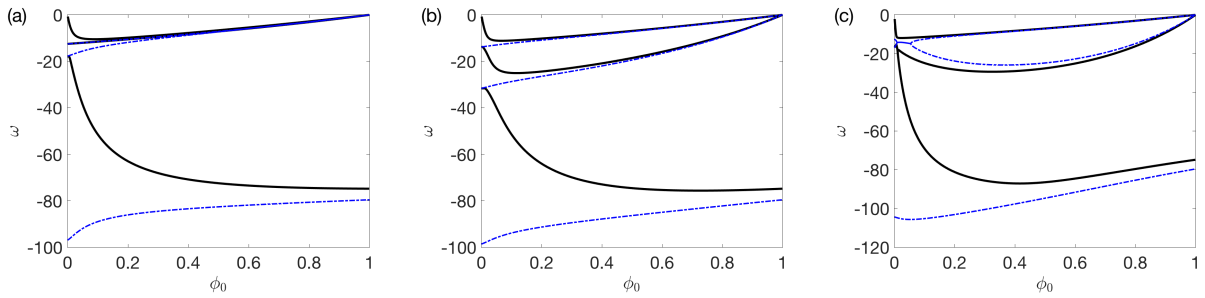

FIG. 9. Eigenvalues ω as a function of ϕ_0 with $\Lambda = 0.5$, $\mu_s = 10^{-2}$ and $\xi = 10^{-2}$. (a) $\beta = 0$ and $\eta = 0$. (b) $\beta = 1$ and $\eta = 0$. (c) $\beta = 0$ and $\eta = 1$.

for Equation (75). We can not find any indication of complex roots for the full nonlinear eigenvalue problem with the same parameter values. Our computation also shows that all eigenvalues of Equation (75) are negative, implying that the steady equilibrium solutions that we found are stable.

IV. CONCLUSIONS AND ONGOING RESEARCH

In this work we develop a two-phase flow model for a poroelastic fluid that consists of an elasco-viscous network fully immersed in a viscous fluid. This model is equivalent to the incompressible Brinkmann equations when the network is rigid and does not move in the reference frame. If the viscous dissipation in the poroelastic fluid is sub-dominated by the pressure gradient force and the friction force, our two-phase flow model is reduced to Darcy fluid with a deformable network phase. Appropriate boundary conditions at the boundary between the biphasic poroelastic fluid and a viscous Stokes flow are derived by the free energy dissipation principle.

Applying this model to the small-deformation dynamics of a poroelastic drop under linear flows, we are able to find steady equilibrium solutions and examine the effects of interfacial slip and permeability on the flow around the drop. Under a uniaxial extensional flow, non-zero interfacial permeability gives rise to an interior flow of similar pattern while the exterior flow around the interface depends a lot on the interfacial slip. Under a planar shear flow, the network rotates with the vorticity in the shear flow and such a rigid-body rotation is the dominant interior flow at a steady equilibrium in the absence of permeability. Different flow patterns develop around the drop due to the combination of permeability and slip.

The kinematic boundary condition for a poroelastic drop governs the interface moving with the normal component of the network velocity at the interface. This renders the eigenvalue problem nonlinear and we are able to compute the first three roots and compare them with an approximated linear eigenvalue system. We find that the eigenvalues are the same for both extensional and shear flow, and all the eigenvalues are negative. These are similar to the small-deformation dynamics of a viscous drop in linear flows.

In the small-deformation limit we assume that the unperturbed volume fraction for the fluid phase is homogeneous. This simplification avoids the complication of having to solve a

linear system of variable-coefficient boundary value equations. In addition this simplification greatly reduces the porosity dependence on the volume fraction. Based on results from MacMinn *et al.*[12] a nonhomogeneous initial volume fraction and a more complicated porosity may not alter the linear dynamics and steady equilibria significantly.

Although our two-phase flow model does not capture the complexity of many biological poroelastic fluids of interest, one expectation is that this approach can be generalized to consider more complex situations such as the swelling and drying due to chemical reaction, polyelectrolytic properties of the solvents in gel-like solutions, and the nonlinear elastohydrodynamics when the displacement amplitude is large. These are all promising directions that we plan to apply our model to after we validate our small-deformation results by comparing against direct numerical simulation results. Currently we are conducting the small-deformation analysis on a soft Brinkman drop (that may be more appropriate for low volume fraction $\phi_s < 5\%$, see the derivations in Caflisch and Rubinstein[1]) in linear flows.

ACKNOWLEDGMENTS

YNY would like to acknowledge helpful discussions with M. Shelley. The authors acknowledge support from NSF-DMS 1614863 and 1412789 (YNY), NSF-DMS 1516978 and 1620316 (YM) and NSF-DMS 1716144 (MJM).

Appendix A: Steady Equilibrium under a Uniaxial Extensional Flow

For a poroelastic drop at the steady equilibrium under a uniaxial extensional flow, the coefficients are

$$d_1 = -\frac{50(4\beta+1)\eta\xi}{7(1-\Lambda)(5\beta\eta\xi\phi_0 - 5\beta\eta\xi - 48\beta\eta\phi_0 - 10\beta\phi_0 + 2\eta\xi\phi_0 - 2\eta\xi - 24\eta\phi_0 - 4\phi_0)}, \tag{A1}$$

$$d_2 = \frac{N_{d_2}}{D_{d_2}}, \tag{A2}$$

$$\begin{aligned} N_{d_2} =& 15(40\beta\eta\Lambda\xi\phi_0 - 40\beta\eta\Lambda\xi + 24\beta\eta\xi\phi_0 - 24\beta\eta\xi - 72\beta\Lambda\phi_0 - 56\beta\phi_0 + \\ & 13\eta\Lambda\xi\phi_0 - 13\eta\Lambda\xi - 48\eta\Lambda\phi_0 + 6\eta\xi\phi_0 - 6\eta\xi - 24\Lambda\phi_0 - 14\phi_0), \\ D_{d_2} =& (1-\Lambda)(12\Lambda+7)(\phi_0-1)(5\beta\eta\xi\phi_0 - 5\beta\eta\xi - 48\beta\eta\phi_0 - 10\beta\phi_0 + \\ & 2\eta\xi\phi_0 - 2\eta\xi - 24\eta\phi_0 - 4\phi_0), \end{aligned}$$

$$d_3 = \frac{N_{d_3}}{D_{d_3}}, \tag{A3}$$

$$\begin{aligned} N_{d_3} =& 9(3\Lambda+7)(-32\beta\eta\Lambda\xi\phi_0 + 32\beta\eta\Lambda\xi - 32\beta\eta\xi\phi_0 + 32\beta\eta\xi + 280\beta\phi_0 - \\ & 8\eta\Lambda\xi\phi_0 + 8\eta\Lambda\xi + 27\eta\xi\phi_0 - 27\eta\xi - 560\eta\phi_0), \\ D_{d_3} =& 7D_{d_2}, \end{aligned}$$

$$A_1 = \frac{10(\beta\eta\xi\phi_0 - \beta\eta\xi + 16\beta\eta\phi_0 - 2\beta\phi_0 + \eta\xi\phi_0 - \eta\xi - 8\eta\phi_0 - 2\phi_0)}{5\beta\eta\xi\phi_0 - 5\beta\eta\xi - 48\beta\eta\phi_0 - 10\beta\phi_0 + 2\eta\xi\phi_0 - 2\eta\xi - 24\eta\phi_0 - 4\phi_0}, \tag{A4}$$

$$A_2 = -\frac{6(16\beta\eta\phi_0 + \eta\xi\phi_0 - \eta\xi - 12\eta\phi_0 - 2\phi_0)}{5\beta\eta\xi\phi_0 - 5\beta\eta\xi - 48\beta\eta\phi_0 - 10\beta\phi_0 + 2\eta\xi\phi_0 - 2\eta\xi - 24\eta\phi_0 - 4\phi_0}. \tag{A5}$$

Appendix B: Steady Equilibrium under a Planar Shear Flow

For a poroelastic drop at the steady equilibrium under a planar shear flow, the coefficients are

$$C_1 = -\frac{10(\beta\eta\xi(\phi_0-1) + 16\beta\eta\phi_0 - 2\phi_0(\beta+4\eta) + \eta\xi(\phi_0-1) - 2\phi_0)}{5\beta\eta\xi(\phi_0-1) - 48\beta\eta\phi_0 - 2\phi_0(5\beta+12\eta) + 2\eta\xi(\phi_0-1) - 4\phi_0}, \tag{B1}$$

$$C_3 = \frac{5(16\beta\eta\phi_0 + \eta\xi(\phi_0-1) - 12\eta\phi_0 - 2\phi_0)}{5\beta\eta\xi(\phi_0-1) - 48\beta\eta\phi_0 - 2\phi_0(5\beta+12\eta) + 2\eta\xi(\phi_0-1) - 4\phi_0}, \tag{B2}$$

$$d_1 = \frac{10(4\beta+1)\eta\xi(\phi_0-1)}{-5\beta\eta\xi(\phi_0-1) + 48\beta\eta\phi_0 + 2\phi_0(5\beta+12\eta) - 2\eta\xi(\phi_0-1) + 4\phi_0}, \tag{B3}$$

$$d_3 = \frac{N_{d_3}}{D_{d_3}}, \tag{B4}$$

$$\begin{aligned} N_{d_3} =& -5(2(20\beta\eta\Lambda\xi(\phi_0-1) + 12\beta\eta\xi(\phi_0-1) - 12\Lambda\phi_0 - 7\phi_0) - \\ & 8\phi_0(9\beta\Lambda + 7\beta + 6\eta\Lambda) + \eta(13\Lambda+6)\xi(\phi_0-1)), \\ D_{d_3} =& (1-\Lambda)(12\Lambda+7)(\phi_0-1)(5\beta\eta\xi(\phi_0-1) - 48\beta\eta\phi_0 - 2\phi_0(5\beta+12\eta) + 2\eta\xi(\phi_0-1) - 4\phi_0), \end{aligned}$$

$$d_4 = \frac{3(3\Lambda+7)(32\beta\eta(\Lambda+1)\xi(\phi_0-1) - 280\phi_0(\beta-2\eta) - \eta(27-8\Lambda)\xi(\phi_0-1))}{7D_{d_3}}. \tag{B5}$$

Appendix C: Linear solutions under a Uniaxial Extensional Flow

$$\mathbf{v}_{s,1}\cdot\hat{\mathbf{r}} = \frac{h_0(r)}{3}\left(1+3\cos(2\theta)\right)e^{\omega t}, \tag{C1}$$

$$\mathbf{v}_{s,1}\cdot\hat{\theta} = h_1(r)\sin(2\theta)e^{\omega t}, \tag{C2}$$

$$p_1 = \frac{(1-\phi_0)}{12r}\left[(8(1+\omega\mu_s)h_0 + 2(1+\Lambda+\omega\mu_s)rh_0' + \right. \tag{C3}$$
$$\left.\left(12(1+\omega\mu_s)h_1 - 2(1-\Lambda+\omega\mu_s)rh_1' - 2(1-\Lambda+\omega\mu_s)r^2h_1''\right)\right]\left(1+3\cos(2\theta)\right)e^{\omega t},$$

$$h_0 = \alpha_1 r + \alpha_3 r^3 + \alpha_5 g_1(r), \tag{C4}$$

$$h_1 = -\alpha_1 r - \frac{5}{3}\alpha_3 r^3 + \alpha_5 g_2(r), \tag{C5}$$

$$\psi_{e,1} = \left(\frac{a_1}{2} - \frac{a_2}{2r^2}\right)\cos\theta\sin^2\theta e^{\omega t}, \tag{C6}$$

$$P_1 = -\frac{\alpha_e}{2r^3}a_1\left(1+3\cos(2\theta)\right)e^{\omega t}. \tag{C7}$$

Appendix D: Linear solutions under a Planar Shear Flow

$$\mathbf{v}_{s,1}\cdot\hat{\mathbf{r}} = f_0(r)\sin^2\theta\sin(2\phi)e^{\omega t}, \tag{D1}$$

$$\mathbf{v}_{s,1}\cdot\hat{\theta} = \frac{f_1(r)}{2}\cos(2\theta)\sin(2\phi)e^{\omega t}, \tag{D2}$$

$$\mathbf{v}_{s,1}\cdot\hat{\phi} = f_1(r)\sin\theta\cos(2\phi)e^{\omega t}, \tag{D3}$$

$$p_1 = \frac{(1-\phi_0)}{4r}\left[(8(1+\omega\mu_s)f_0 + 2(1+\Lambda+\omega\mu_s)rf_0' - \right. \tag{D4}$$
$$\left.\left(12(1+\omega\mu_s)f_1 - 2(1-\Lambda+\omega\mu_s)rf_1' - 2(1-\Lambda+\omega\mu_s)r^2f_1''\right)\right]\left(1+3\cos(2\theta)\right)e^{\omega t},$$

$$f_0 = \alpha_1 r + \alpha_3 r^3 + \alpha_5 g_1(r), \tag{D5}$$

$$f_1 = \alpha_1 r + \frac{5}{3}\alpha_3 r^3 - \alpha_5 g_2(r), \tag{D6}$$

$$\mathbf{U}_1\cdot\hat{\mathbf{r}} = \frac{1}{20r^4}\left(c_3 + 5c_1r^2\right)\sin^2\theta\sin(2\phi)e^{\omega t}, \tag{D7}$$

$$\mathbf{U}_1\cdot\hat{\theta} = -\frac{1}{10r^4}c_3\sin(2\theta)\sin(2\phi)e^{\omega t}, \tag{D8}$$

$$\mathbf{U}_1\cdot\hat{\phi} = -\frac{1}{10r^4}\left(10c_4r^2 + 2c_3\cos(2\phi)\right)\sin\theta e^{\omega t}, \tag{D9}$$

$$P_1 = \frac{\alpha_e}{2r^3}c_1\sin^2\theta\sin(2\phi)e^{\omega t}. \tag{D10}$$

---

[1] R. E. Caflisch and J. Rubinstein, "Chapter 6: Flow in porous media," in *Lectures on the mathematical theory of multi-phase flow* (New York University, 1986).

[2] Seung-Man Yang and Won-Hi Hong, "Motions of a porous particle in stokes flow: part 1. unbounded single-fluid domain problem," Korean J. Chem. Eng. **5**, 23–34 (1988).

[3] Seung-Man Yang and Won-Hi Hong, "Motions of a porous particle in stokes flow: part 2. unbounded single-fluid domain problem," Korean J. Chem. Eng. **6**, 234–245 (1989).

[4] Seung-Man Yang and L. Gary Leal, "Motions of a porous particle in stokes flow near a plane-fluid interface," Physicochemical Hydrodynamics **11**, 543–569 (1989).

[5] R. H. Davis and H. A. Stone, "Flow through beds of porous particles," Chem. Eng. Sci. **48**, 3993–4005 (1993).

[6] L. Gary Leal, "Chapter 8: Creeping flow - three-dimensional problems," in *Advanced Transport Phenomena* (Cambridge University Press, 2007).

[7] E. Holland and R. E. Showalter, "Poro-visco-elastic compaction in sedimentary basins," SIAM J. Math. Anal. **50**, 2295–2316 (2018).

[8] F. A. Morales and R. E. Showalter, "A darcy-brinkman model of fractures in porous media," J. Math. Anal. Appl. **452**, 1332–1358 (2017).

[9] L. Bociu, G. Guidoboni, R. Sacco, and J. T. Webster, "Analysis of nonlinear poro-elastic and poro-visco-elastic models," Arch. Rational Mech. Anal. **222**, 1445–1519 (2016).

[10] H. T. Banks, K. Bekele-Maxwell, L. Bociu, M. Noorman, and G. Guidoboni, "Sensitivity analysis in poro-elastic and poro-visco-elastic models with respect to boundary data," Quaterly of Applied Mathematics **4**, 697–735 (2017).

[11] M. Verri, G. Guidoboni, L. Bociu, and R Sacco, "The role of structural viscoelasticity in deformable porous media with incompressible constituents: applications in biomechanics," Math. Biosci. Eng. **15**, 939–959 (2018).

[12] C. W. MacMinn, E. R. Dufresne, and J. S. Wettlaufer, "Large deformation of a soft porous material," Phys. Rev. Applied **5**, 044020 (2016).

[13] W. M. Lai, J. S. Hou, and V. C. Mow, "A triphasic theory for the swelling and deformation behaviors of articular cartilage," J. Biomech. Eng. **113**, 245–258 (1991).

[14] P. M. Pinsky, "Three-dimensional modeling of metabolic species transport in the cornea with a hydrogel intrastromal inlay," Invest Ophthalmol Vis. Sci. **55**, 3093–3106 (2014).

[15] X. Chen, S. J. Petsche, and P. M. Pinsky, "A structural model for the in vivo human cornea including collagen-swelling interaction," J. R. Soc. Interface **12**, 20150241 (2015).

[16] P. M. Pinsky and X. Cheng, "A constitutive model for swelling pressure and volumetric behavior of highly-hydrated connective tissue," J. Elast. **129**, 145–170 (2017).

[17] N. G. Cogan and J. P. Keener, "The role of the biofilm matrix in structural development," Math. Med. Biol. **21**, 147–166 (2004).

[18] Y. Mori, H. Chen, C. Micek, and M.-C. Calderer, "A dynamic model of polyelectrolyte gels," SIAM J. Appl. Math. **73**, 103–133 (2013).

[19] S. Saleh, J. F. Thovert, and P. M. Adler, "Flow along porous media by particle image velocimetry," AIChE Journal **39**, 1765–1776 (1993).

[20] P. Angot, B. Goyeau, and J. A. Ochoa-Tapia, "Asymptotic modeling of transport phenomena at the interface between a fluid and a porous layer: Jump conditions," Phys. Rev. E **95**, 063302 (2017).

[21] G. S. Beavers and D. D. Joseph, "Boundary conditions at a naturally permeable wall," J. Fluid Mech. **30**, 197–207 (1967).

[22] P. Angot, G. Carbou, and V. Peron, "Asymptotic study for Stokes-Brinkman model with jump embedded transmission conditions," Asymptotic Analysis **96**, 223–249 (2016).

[23] P. Angot, "On the well-posed coupling between free fluid and porous viscous flows," Applied Math. Lett. **24**, 803–810 (2011).

[24] J. A. Ochoa-Tapia, "Momentum transfer at the boundary between a porous medium and a homogeneous fluid - ii. comparison with experiment," Int. J. Heat Mass Transfer **38**, 2647–2655 (1995).

[25] D. R. Hewitt, J. S. Nijjer, and M. G. Worster, "Flow-induced compaction of a deformable porous medium," Phys. Rev. E **93**, 023116 (2016).

[26] M. L. Bars and M. G. Worster, "Interfacial conditions between a pure fluid and a porous medium: implications for binary alloy solidification," J. Fluid Mech. **550**, 149–173 (2006).

[27] P. G. Saffman, "On the boundary condition at the surface of a porous medium," Studies Applied Math. **2**, 93–101 (1971).

[28] G. Neale and W. Nader, "Creeping flow relative to permeable spheres," Chem. Eng. Sci. **28**, 1865–1874 (1973).

[29] G. Neale and W. Nader, "Practical significance of Brinkman's extension of Darcy's law: coupled parallel flows within a channel and a bounding porous medium," Can. J. Chem. Eng. **52**, 475–478 (1974).

[30] E. I. Saad, "Stokes flow past an assemblage of axisymmetric porous spherical shell-in-cell models: effect of stress jump condition," Meccanica **48**, 1747–1759 (2013).

[31] E. I. Saad and M. S. Faltas, "Slow motion of a porous sphere translating along the axis of a circular cylindrical pore subject to a stress jump condition," Transp. Porous Med. **102**, 91–109 (2014).

[32] E. I. Saad, "Axisymmetric motion of a porous sphere through a spherical envelop subject to a stress jump condition," Meccanica **51**, 799–817 (2016).

[33] U. Lacis, G. A. Zampogna, and S. Bagheri, "A computational continuum model of poroelastic beds," Proc. R. Soc. A , 20160932 (2017).

[34] U. Lacis and S. Bagheri, "A framework for computing effective boundary conditions at the interface between fluid and a porous medium," J. Fluid Mech. **812**, 866–889 (2017).

[35] G. Dagan, "The generalization of Darcy's law for nonuniform flows," Water Resources Research **15**, 1–7 (1979).

[36] W. Jager and A. Mikelic, "Modeling effective interface laws for transport phenomena between an unconfined fluid and a porous medium using homogenization," Transp. Porous Med. **78**, 489–508 (2009).

[37] T. Carraro, C. Goll, A. Marciniak-Czochra, and A. Mikelic, "Pressure jump interface law for the stokes-darcy coupling: confirmation by direct numerical simulations," J. Fluid Mech. **732**, 510–536 (2013).

[38] S. Haber and R. Mauri, "Boundary conditions for darcy's flow through porous media," Int. J. Multiphase Flow **9**, 561–574 (1983).

[39] E. Lauga, M. P. Brenner, and H. A. Stone, "Microfluidics: The no-slip boundary condition," in *Handbook of Experimental Fluid Dynamics*, edited by C. Tropea, A. Yarin, and J. F. Foss (Springer, New York, 2007).

[40] H. J. Keh and Y. C. Chang, "Creeping motion of a slip spherical particle in a circular cylindrical pore," Int. J. Multiphase Flow **33**, 726–741 (2007).

[41] See supplementary material at https:// for entries of the matrixes **A** and **B**., .